Supplementary material

Section 1 Supplementary figures

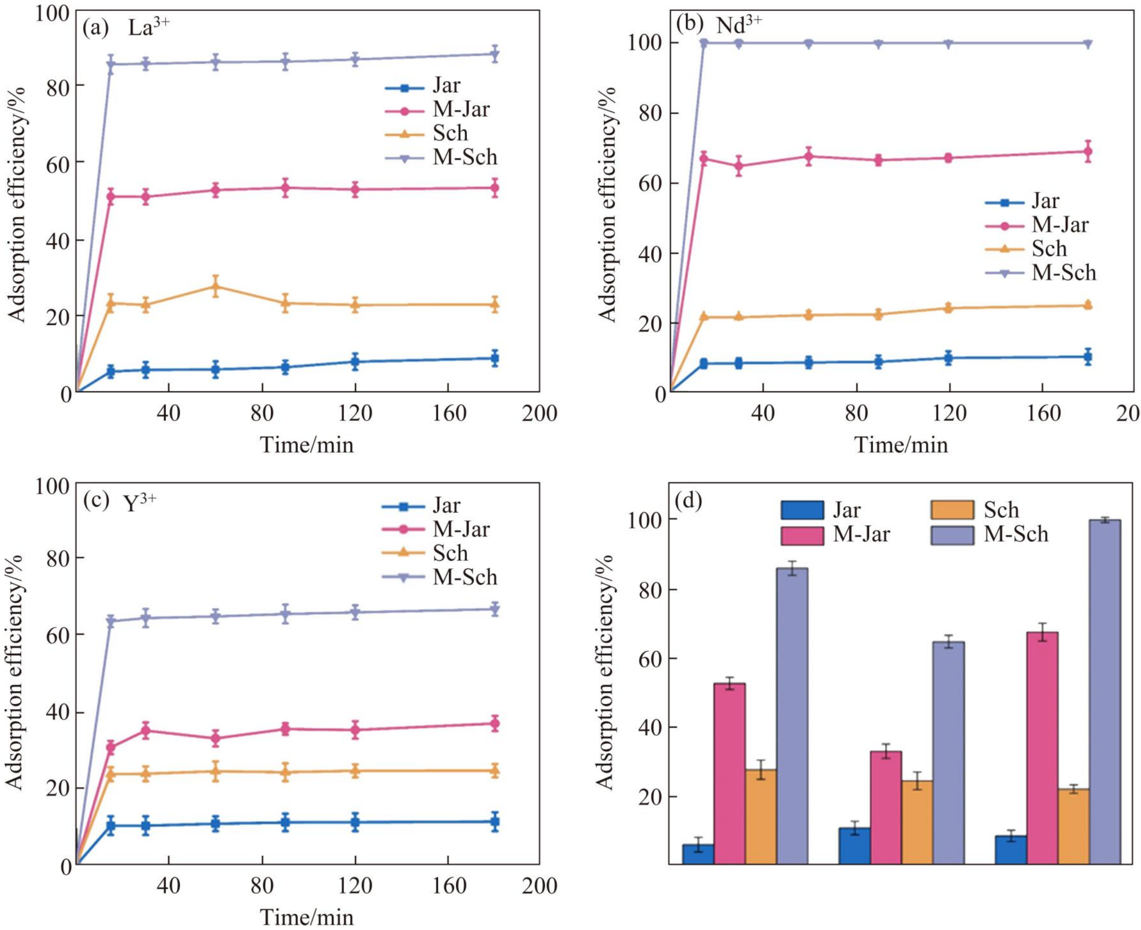

Figure S1 The adsorption efficiency of different materials (Jar, Sch, M-Jar, M-Sch) for (a) La^{3+}, (b) Nd^{3+}, and (c) Y^{3+} varies with different exposure time; (d) The adsorption efficiency of La^{3+}, Nd^{3+} and Y^{3+} adsorbed by different materials for 1 h (Conditions: initial concentrations of La^{3+}, Nd^{3+} and Y^{3+} were 5 mg/L, the adsorbent dose was 50 mg, room temperature, pH=6, and V=50 mL)

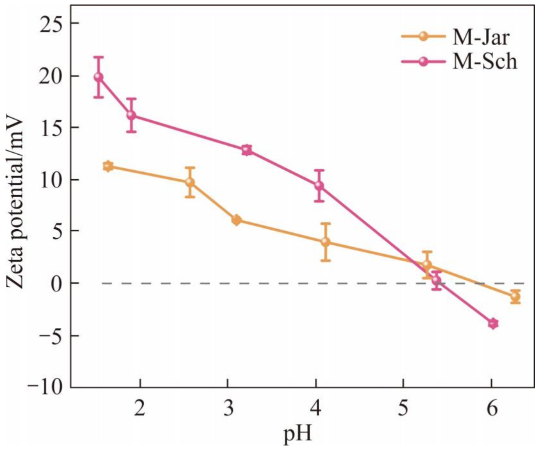

Figure S2 Zeta potential of M-Jar and M-Sch at different pH

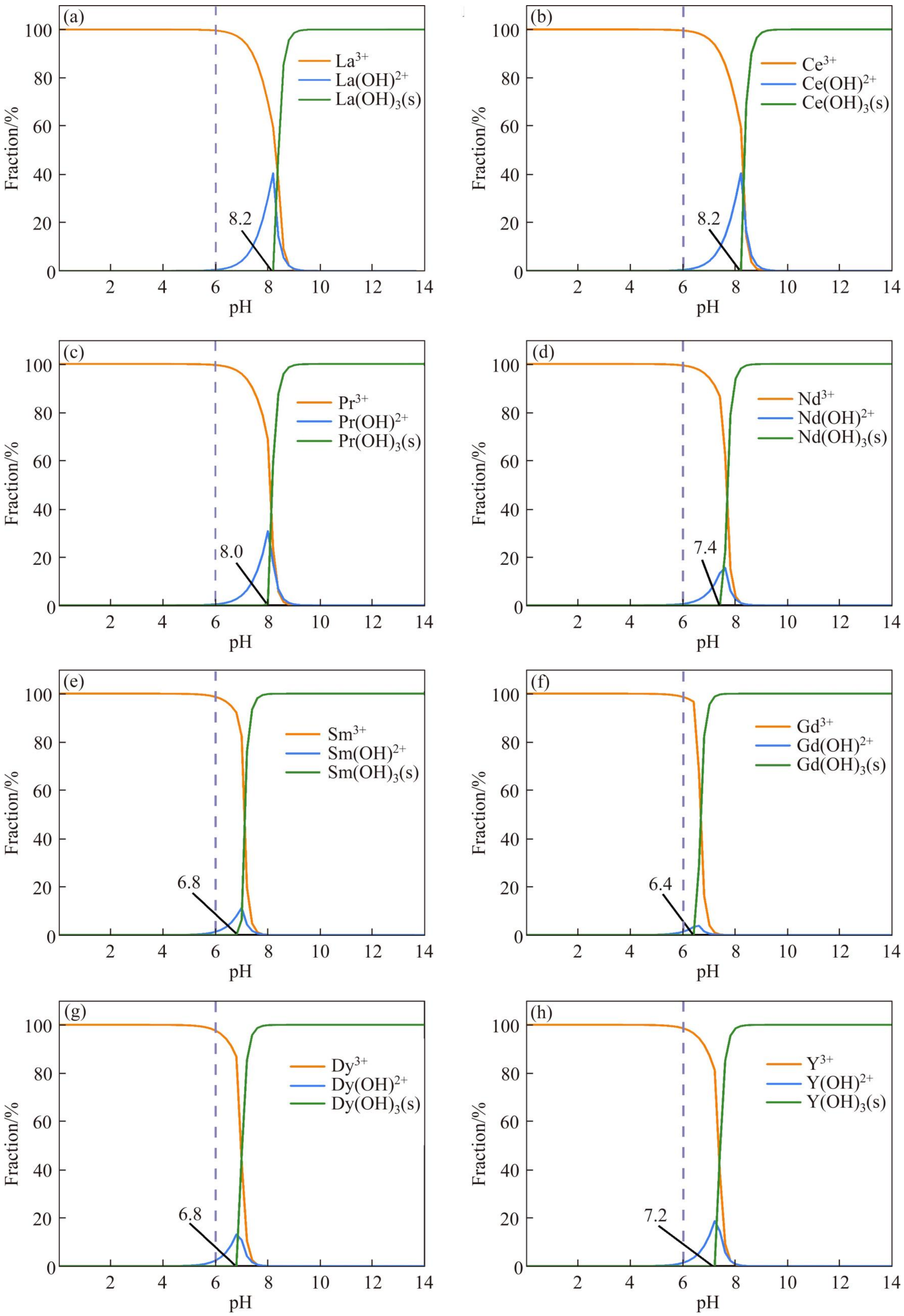

Figure S3 Species distribution of hydrolysis products of RE^{3+} in aqueous solution as a function of pH value (Conditions: initial concentration of RE^{3+}=5 mg/L, 25 °C

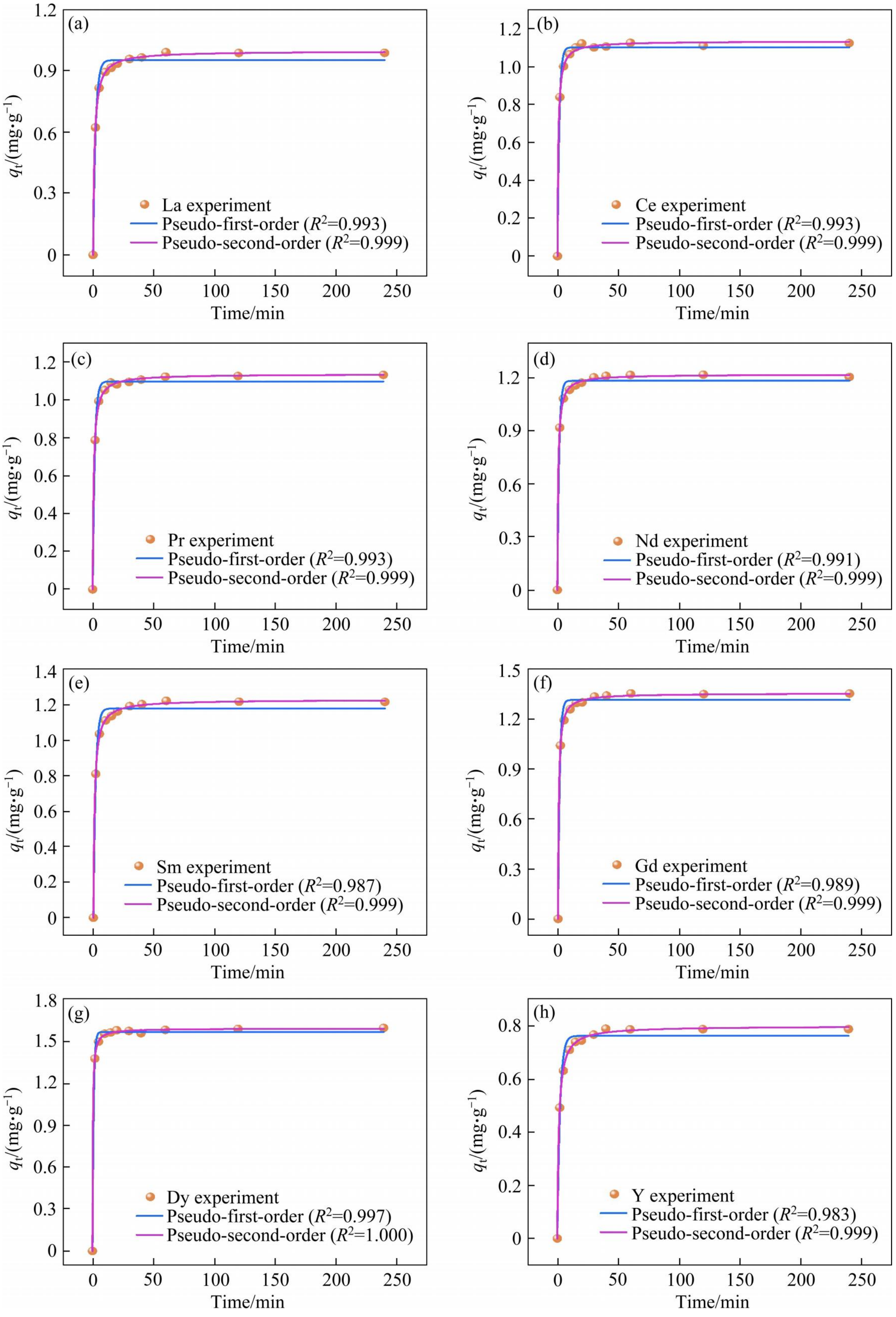

Figure S4 The pseudo-first-order and pseudo-second-order fitting of the adsorption data on M-Jar (Conditions: initial concentrations of RE^{3+}=5 mg/L, the adsorbent dose was 50 mg, room temperature, V=50 mL, pH=5): (a) La; (b) Ce; (c) Pr; (d) Nd; (e) Sm; (f) Gd; (g) Dy; (h) Y

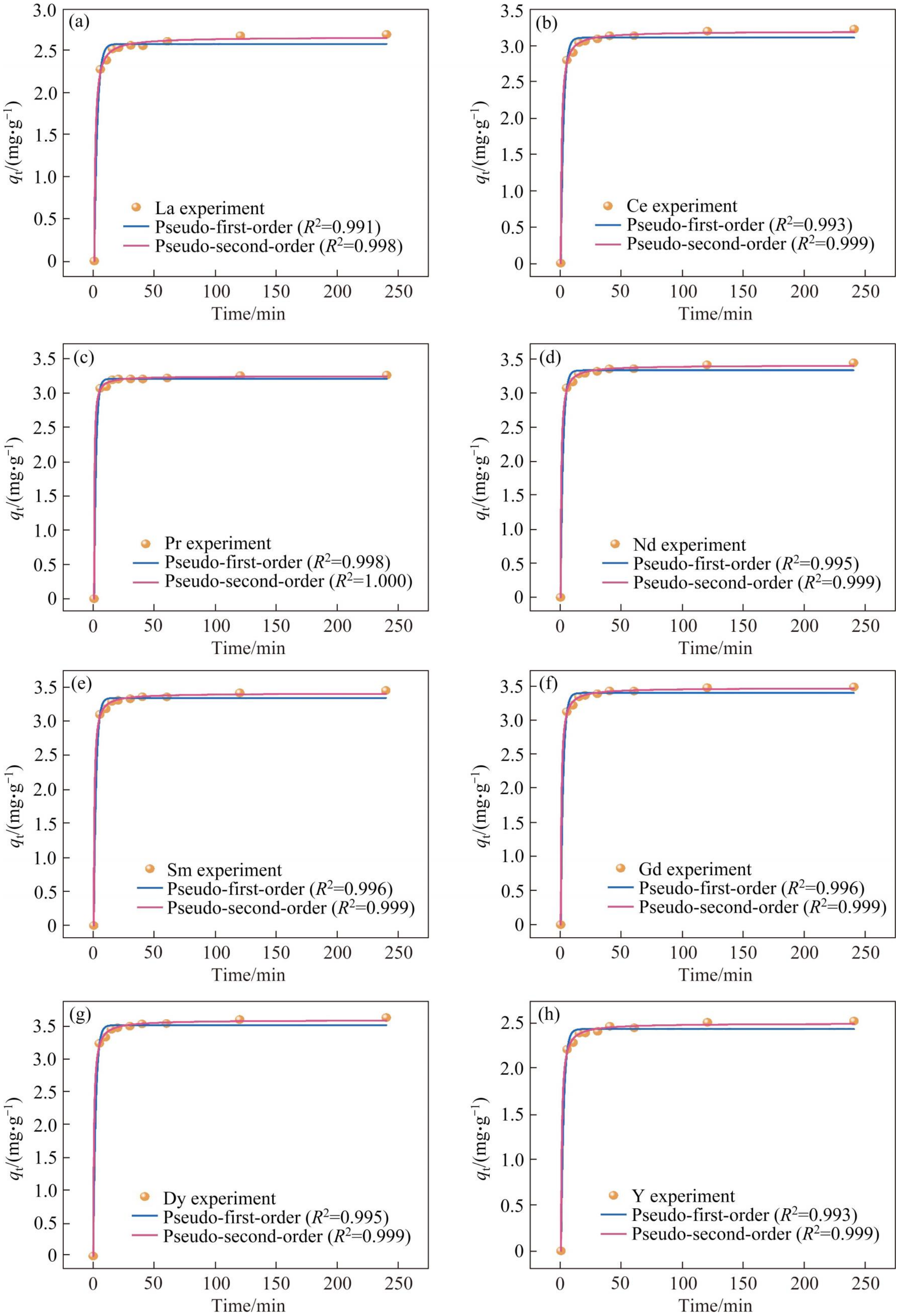

Figure S5 The pseudo-first-order and pseudo-second-order fitting of the adsorption data on M-Sch (Conditions: initial concentrations of RE^{3+}=5 mg/L, the adsorbent dose was 50 mg, room temperature, *V*=50 mL, pH=5): (a) La; (b) Ce; (c) Pr; (d) Nd; (e) Sm; (f) Gd; (g) Dy; (h) Y

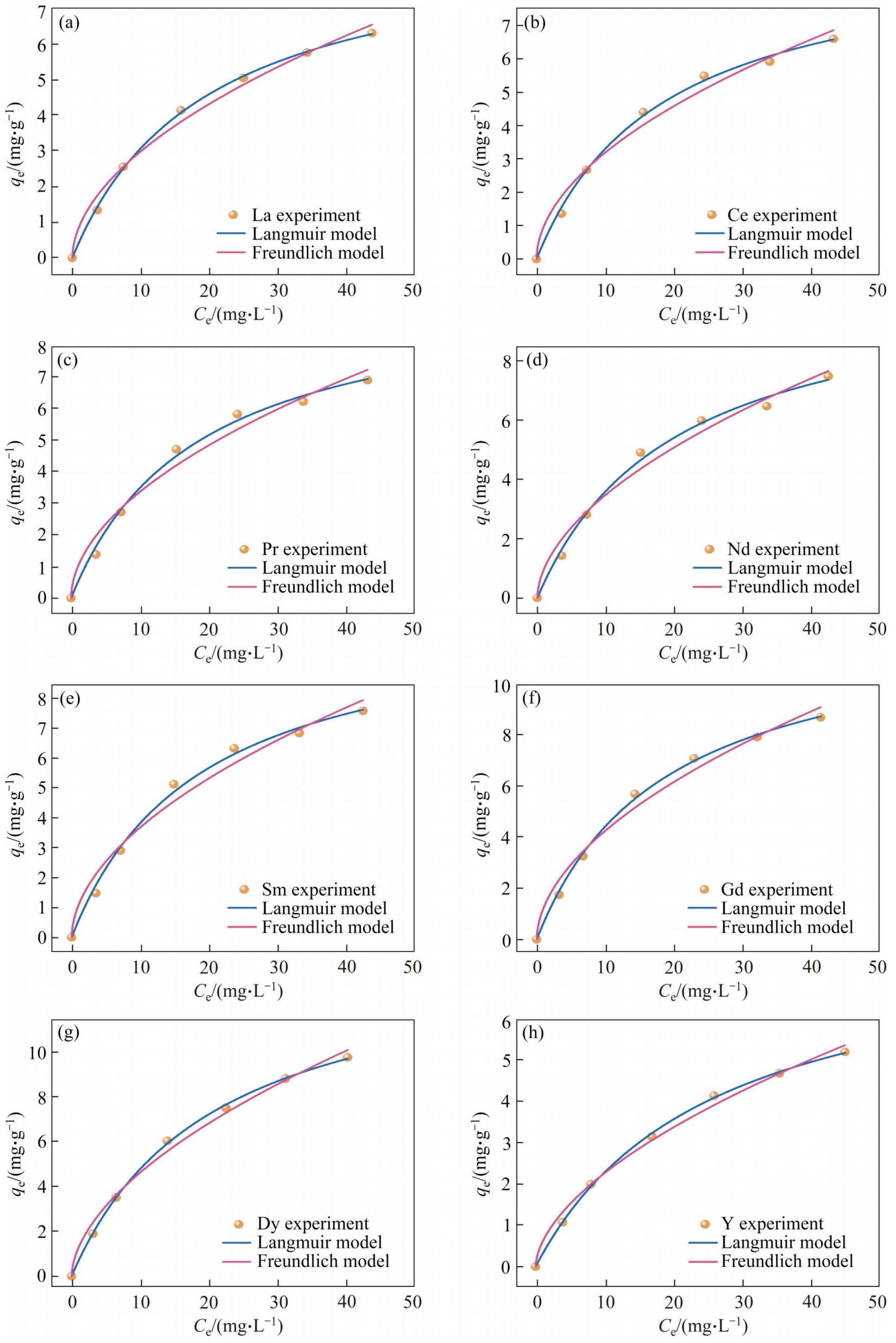

Figure S6 The adsorption data of RE^{3+} onto M-Jar fitting by Langmuir and Freundlich isotherm models (Conditions: initial concentrations of RE^{3+} were 5−50 mg/L, the adsorbent dose was 50 mg, room temperature, V=50 mL, pH=6): (a) La; (b) Ce; (c) Pr; (d) Nd; (e) Sm; (f) Gd; (g) Dy; (h) Y

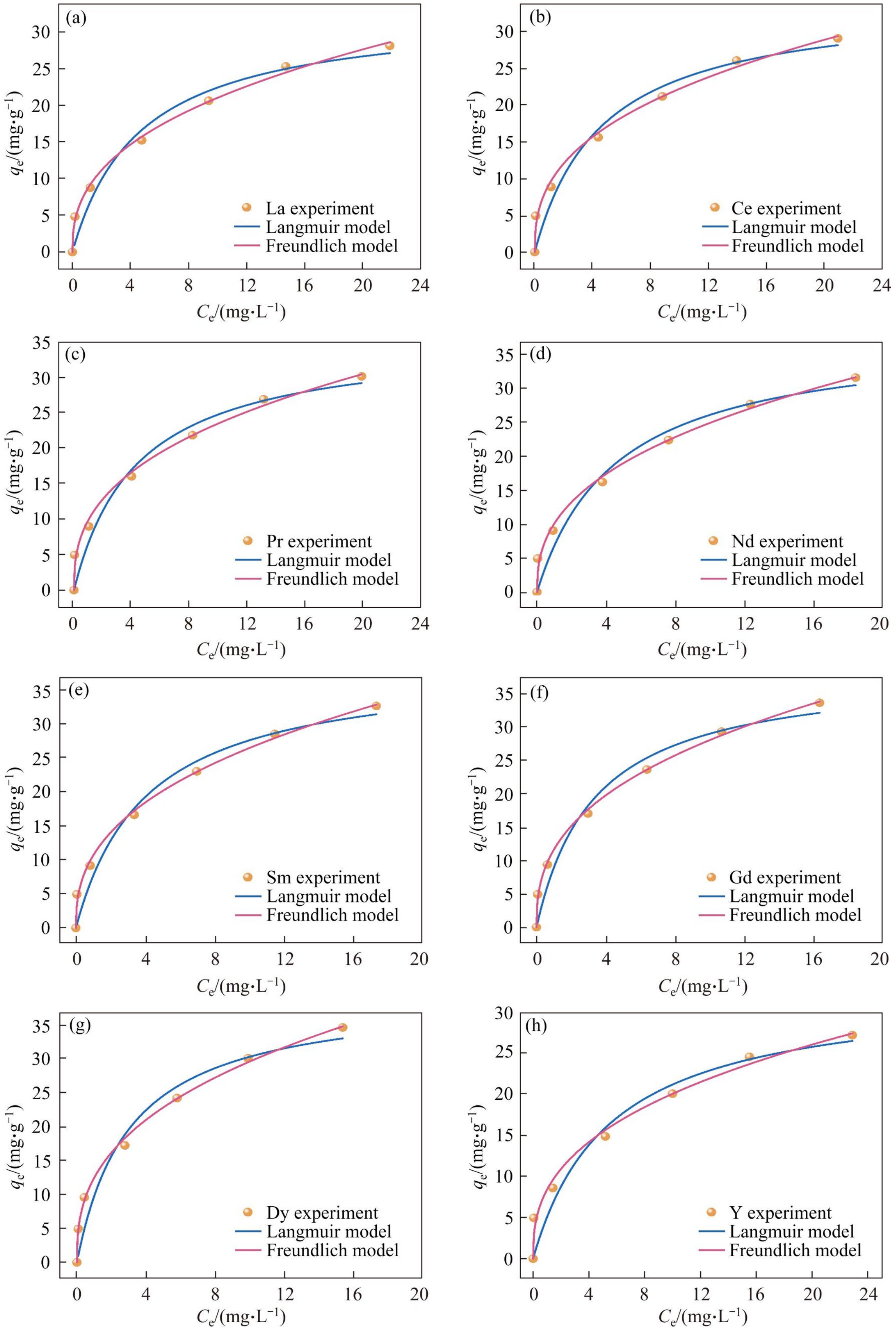

Figure S7 The adsorption data of RE^{3+} onto M-Sch fitting by Langmuir and Freundlich isotherm models (Conditions: initial concentrations of RE^{3+} were 5−50 mg/L, the adsorbent dose was 50 mg, room temperature, V=50 mL, pH=6): (a) La; (b) Ce; (c) Pr; (d) Nd; (e) Sm; (f) Gd; (g) Dy; (h) Y

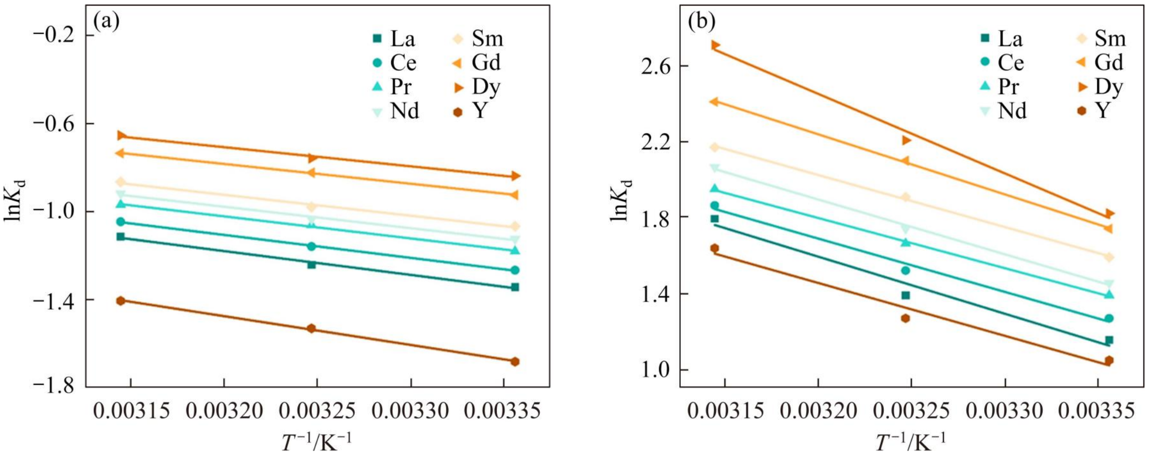

Figure S8 Linear plot of $\ln K_d$ versus $1/T$ for adsorption capacity of RE^{3+} on (a) M-Jar and (b) M-Sch (Conditions: initial concentrations of RE^{3+}=20 mg/L, the adsorption dose=50 mg, t=1 h, V=50 mL, pH=6)

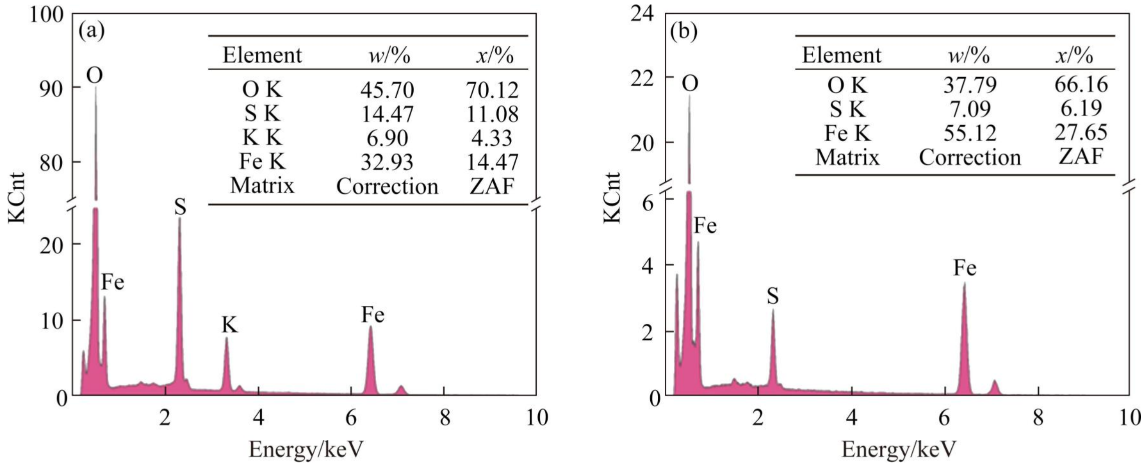

(a)

Element	w/%	x/%
O K	45.70	70.12
S K	14.47	11.08
K K	6.90	4.33
Fe K	32.93	14.47
Matrix	Correction	ZAF

(b)

Element	w/%	x/%
O K	37.79	66.16
S K	7.09	6.19
Fe K	55.12	27.65
Matrix	Correction	ZAF

Figure S9 The EDS spectra of (a) M-Jar and (b) M-Sch before the adsorption of RE^{3+}

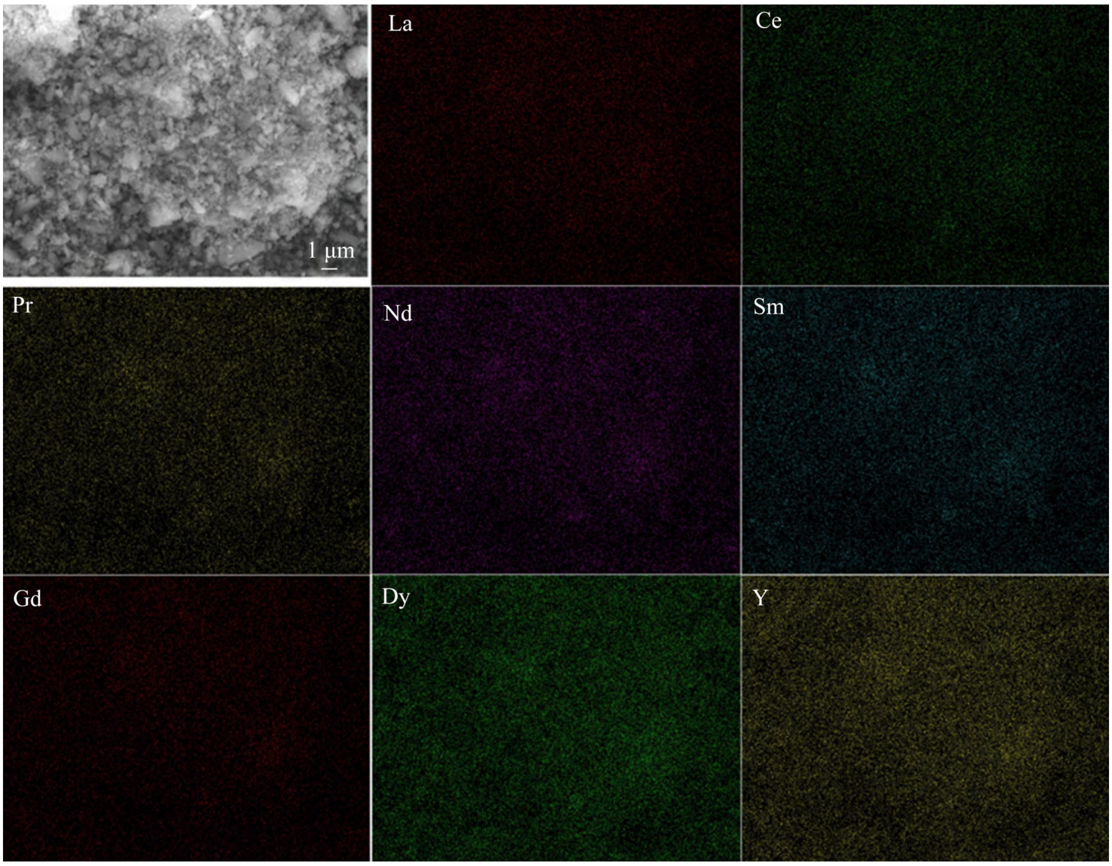

Figure S10 SEM image and elemental mapping of M-Jar after the adsorption of RE^{3+}

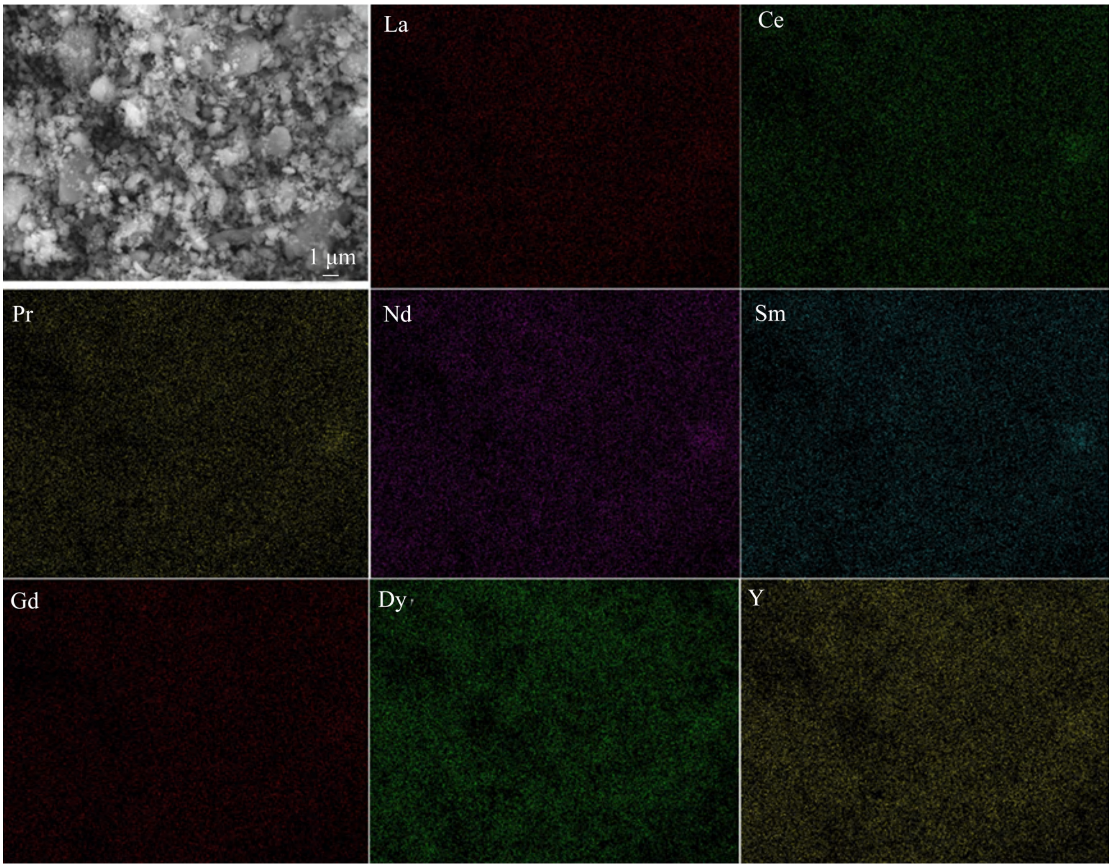

Figure S11 SEM image and elemental mapping of M-Sch after the adsorption of RE^{3+}

Section 2 Supplementary tables

Table S1 Concentrations of various ions in the mine wastewater used in this study

Ions	Concentration/(mg·L^{-1})	Ions	Concentration/(mg·L^{-1})	Ions	Concentration/(mg·L^{-1})
Y	3.019	Pr	0.356	Na	7.502
La	1.630	Sm	0.341	Mg	5.982
Nd	1.461	Ce	0.327	Al	3.060
Dy	0.432	Ca	34.884	Mn	2.025
Gd	0.399	K	11.151		

Table S2 Reported literature review of mixed RE^{3+} adsorption capacities by different adsorbents

Adsorbents	Ions	Adsorption capacity/(mg·g^{-1})	Adsorbent dose/(g·L^{-1})	Ions concentration/ (mg·L^{-1})	Adsorption time/h	Ref.
DTPADA-SBA-15	Eu, Tb, Gd, Sm, Nd	32.1, 31.4, 29.1, 28.5, 25.7	2.5	10.0−500.0	3.0	[1]
Magnetite nanoparticles functionalized with organophosphorus compounds	La, Pr, Nd	8.3, 8.7, 8.9	2.5	1.0−90.0	0.5	[2]
Calcium alginate/carboxymethyl chitosan/$Ni_{0.2}Zn_{0.2}Fe_{2.6}O_4$	Nd, Tb, Dy	23.2, 24.4, 25.2	1.8	30.0−180.0	0.9	[3]
Functionalized SBA-15	Lu, Y	17.0, 17.9	0.2	2.0−40.0	24.0	[4]
Novel metal ion imprinted xanthan gum-layered double hydroxide nanocomposite	Sc, Nd, Tm, Yb	132.3, 14.0, 18.2, 25.7	3.0	10.0−25.0	1.3	[5]
Graphene oxide-tris(4-aminophenyl) amine composites	Yb, Er, Nd, La, Y	30.9, 26.5, 20.6, 11.2, 10.5	0.3	10.0−70.0	0.7	[6]
M-Jar	La, Ce, Pr, Nd, Sm, Gd, Dy, Y	9.1, 9.4, 9.9, 10.8, 11.0, 1.6, 14.7, 8.1	1.0	5.0−50.0	1.0	This work
M-Sch	La, Ce, Pr, Nd, Sm, Gd, Dy, Y	32.9, 34.4, 35.6, 38.1, 38.7, 38.7, 39.5, 32.7	1.0	5.0−50.0	1.0	This work

Section 3 Materials preparation

Jar preparation: *A. ferrooxidans* (3.5×10^7 cells/mL) was inoculated in 500 mL of a solution of $FeSO_4\cdot7H_2O$ (0.16 mol/L) and K_2SO_4 (26.65 mmol/L) at pH 2.0, and the reaction proceeded for 72 h in a shaking incubator (170 r/min, 30 °C). The formed precipitate was then collected by filtration with Whatman 42 filter paper, and soluble impurities were eliminated by washing triple times with dilute H_2SO_4 solution (pH=2.0) and deionized water. Finally, the precipitate was dried to obtain biosynthetic jarosite for subsequent use [7].

Sch preparation: *A. ferrooxidans* was inoculated in 500 mL of 0.144 mol/L $FeSO_4\cdot7H_2O$, and the pH of the system was maintained at 3.0 by adding dilute H_2SO_4. The other conditions were the same as those used in the preparation of Jar [8].

M-Jar and M-Sch preparations: The aforementioned Jar and Sch were mechanically activated by a planetary ball mill (YXQM-4L, MITR). Briefly, the M-Jar and M-Sch were obtained by adding Jar and Sch to the planetary ball mill tank at a ball-to-material ratio of 20:1, respectively, and milling at 700 r/min for 5 h [9].

Section 4 Adsorption and desorption experiments

Initially, batch adsorption experiments were used to examine the adsorption efficiencies of the four different materials (Jar, Sch, M-Jar, M-Sch) for single RE^{3+}. Each material was exposed to La^{3+}, Nd^{3+}, and Y^{3+} solutions, which were prepared by dissolving $LaCl_3$, $NdCl_3$, and YCl_3 in deionized water. LIU et al [10] found that the concentration of RE^{3+} ranging from 3.84 to 4.33 mg/L in a wastewater sample. Therefore, the same experimental setup was used for all batch comparison experiments: initial RE^{3+} concentration of 5 mg/L, 50 mg adsorbent, pH=6, V=50 mL, and room temperature. The pH was adjusted by adding 0.1 mol/L sodium hydroxide or nitric acid solution [11]. After adsorption, solution samples were taken out and filtered through a 0.22 μm filter membrane to measure the concentration of the remaining RE^{3+} in the solution using inductively coupled plasma mass spectrometry (ICP-MS) [12]. Then, the adsorption capacities of the four different materials for RE^{3+} were evaluated. The results showed that M-Jar and M-Sch exhibited highly promising adsorption properties. Therefore, they were used to adsorb mixed RE^{3+} in the remaining adsorption experiments.

The following adsorption experiments were conducted at room temperature in consideration of the types and concentrations of RE^{3+} in the actual mine wastewater sample: 50 mL of RE^{3+} (La^{3+}, Ce^{3+}, Pr^{3+}, Nd^{3+}, Sm^{3+}, Gd^{3+}, Dy^{3+} and Y^{3+}) mixture solution (5 mg/L each) and 50 mg of adsorbent. The adsorption kinetics were examined by stirring on a magnetic stirrer for 240 min. The effect of pH was explored within the pH range of 2.0 to 7.0 [13]. The procedure for thermodynamic experiments and equilibrium isotherms were the same as described above, except that the temperature range was 25 to 45 °C and the initial RE^{3+} concentration range was defined as 5 to 50 mg/L. All experiments were performed in triplicate. The adsorption efficiency η (%) and the adsorption capacity q_e (mg/g) of the adsorbent were calculated according to Eqs. (1) and (2) [14].

$$\eta = \frac{C_0 - C_e}{C_0} \times 100\% \qquad (1)$$

$$q_e = \frac{(C_0 - C_e)V}{m} \qquad (2)$$

where C_0 (mg/L) and C_e (mg/L) are the initial and equilibrium concentrations of RE^{3+}, respectively; V (L) denotes the volume of the solution, and m (g) stands for the mass of the adsorbent.

For the desorption experiment, the adsorbent loaded with RE^{3+} was desorbed by stirring with 0.5 mol/L HNO_3 for 1 h. Following this, the solid sample was collected by filtering and drying for readsorption. The entire procedure was carried out five times to evaluate the regeneration and reusability of the adsorbent.

Finally, actual IARE mine wastewater was used to assess the adsorption performance of M-Sch. Prior to use, the wastewater was filtered using a 0.22 μm filter and the concentration of metal ions was detected by ICP-MS [12]. The adsorption experiments on the removal of RE^{3+} from the mine wastewater were conducted under the conditions of M-Sch (200 mg), wastewater (50 mL), pH=6, contact time (1 h), and room temperature.

Section 5 Theoretical fundamentals

In this study, pseudo-first-order kinetic model (Eq. (3)) and pseudo-second-order kinetic model (Eq. (4)) were used to analyze the kinetics of M-Jar and M-Sch interactions with RE^{3+} [13].

$$\ln(q_e - q_t) = \ln q_e - k_1 t \qquad (3)$$

$$\frac{t}{q_t} = \frac{1}{k_2 q_e^2} + \frac{t}{q_e} \qquad (4)$$

where q_e (mg/g) and q_t (mg/g) represent the adsorption capacity at equilibrium and time t, respectively; k_1 (min^{-1}) is the pseudo-first-order kinetic rate constant, and k_2 (g/(mg·min)) is the pseudo-second-order kinetic rate constant.

To elucidate the adsorption characteristics of RE^{3+} on M-Jar and M-Sch, two typical isotherm fitting models, Langmuir (Eq. (5)) and Freundlich (Eq. (6)) [13], were used to analyze the experimental equilibrium data.

$$q_e = q_m \frac{K_L C_e}{1 + K_L C_e} \qquad (5)$$

$$q_e = K_F C_e^{1/n} \quad (6)$$

where q_m (mg/g) is the maximum adsorption capacity; K_L (L/mg) and K_F (mg/g) are the Langmuir and the Freundlich constants, respectively; n stands for the Freundlich constant, which indicates the heterogeneity index [15].

In addition, the thermodynamic parameters of Gibbs free energy ΔG^Θ (kJ/mol), enthalpy ΔH^Θ (kJ/mol), and entropy ΔS^Θ (J/(K·mol)) of the adsorption of RE^{3+} on M-Jar and M-Sch were calculated based on Eqs. (7)−(9) [16].

$$\ln K_d = \frac{\Delta S^\Theta}{R} - \frac{\Delta H^\Theta}{RT} \quad (7)$$

$$K_d = \frac{q_e}{C_e} \quad (8)$$

$$\Delta G^\Theta = -RT \ln K_d \quad (9)$$

where K_d (L/g) is the thermodynamic equilibrium constant; R denotes the universal gas constant (8.314 J/(mol·K)); and T (K) represents the temperature.

Section 6 Comparison of sorbent material

The adsorption efficiencies of four materials (Jar, Sch, M-Jar, M-Sch) for single RE^{3+} (La^{3+}, Nd^{3+} and Y^{3+}) were investigated as a function of exposure time (Figure S1). The findings demonstrated that the adsorption efficiencies of Jar for La^{3+}, Nd^{3+} and Y^{3+} were only 9.04%, 10.28%, and 11.47%, respectively, indicating that the adsorption of RE^{3+} by Jar was not significant. After mechanical activation, the adsorption efficiencies of La^{3+}, Nd^{3+} and Y^{3+} by M-Jar were 5.36%, 68.98% and 36.98%, respectively. It was found that mechanical activation considerably improved the adsorption performance of Jar for RE^{3+}. In contrast, Sch exhibited larger adsorption efficiencies than Jar for La^{3+}, Nd^{3+}, and Y^{3+}, measured at 23.01%, 24.92% and 24.71%, respectively. This might be attributed to the larger surface area due to the amorphous structure of Sch, which was conducive to the adsorption of RE^{3+}. This was further confirmed in the following section where the adsorbents were characterized. M-Sch displayed the highest adsorption capacity for La^{3+}, Nd^{3+} and Y^{3+}, with respective adsorption efficiencies of 88.15%, 100.00% and 66.71%. These results indicated that the RE^{3+} adsorption and reactivity of jarosite and schwertmannite were greatly enhanced by mechanical activation. Therefore, M-Jar and M-Sch were employed in the subsequent adsorption experiments of RE^{3+}.

References

[1] CUI Jing-lei, WANG Qian, GAO Jian-ming, et al. The selective adsorption of rare earth elements by modified coal fly ash based SBA-15 [J]. Chinese Journal of Chemical Engineering, 2022, 47: 155−164. DOI: 10.1016/j.cjche.2021.07.0.

[2] MOLINA L, GAETE J, ALFARO I, et al. Synthesis and characterization of magnetite nanoparticles functionalized with organophosphorus compounds and its application as an adsorbent for La (III), Nd (III) and Pr (III) ions from aqueous solutions [J]. Journal of Molecular Liquids, 2019, 275: 178−191. DOI: 10.1016/j.molliq.2018.11.074.

[3] JAVADIAN H, RUIZ M, SASTRE A M. Response surface methodology based on central composite design for simultaneous adsorption of rare earth elements using nanoporous calcium alginate/carboxymethyl chitosan microbiocomposite powder containing $Ni_{0.2}Zn_{0.2}Fe_{2.6}O_4$ magnetic nanoparticles: Batch and column studies [J]. International Journal of Biological Macromolecules, 2020, 154: 937−95. DOI: 10.1016/j.ijbiomac.2020.0.131.

[4] RYU S, FONSEKA C, NAIDU G, et al. Recovery of rare earth elements (Lu, Y) by adsorption using functionalized SBA-15 and MIL-101 (Cr) [J]. Chemosphere, 2021, 281: 130869. DOI: 10.1016/j.chemosphere.2021.130869.

[5] IFTEKHAR S, SRIVASTAVA V, HAMMOUDA S B, et al. Fabrication of novel metal ion imprinted xanthan gum-layered double hydroxide nanocomposite for adsorption of rare earth elements [J]. Carbohydrate Polymers, 2018, 194: 274−284. DOI: 10.1016/j.carbpol.2018.04.054.

[6] ZHAO Xiao-ru, JIANG Xin-yu, PENG Dong-ming, et al. Behavior and mechanism of graphene oxide-tris(4-aminophenyl)amine

composites in adsorption of rare earth elements [J]. Journal of Rare Earths, 2021, 39(1): 90−97. DOI: 10.1016/j.jre.2020.0.006.

[7] YANG Bao-jun, LIN Mo, FANG Jing-hua, et al. Combined effects of jarosite and visible light on chalcopyrite dissolution mediated by Acidithiobacillus ferrooxidans [J]. Science of the Total Environment, 2020, 698: 134175. DOI: 10.1016/j.scitotenv.2019.134175.

[8] FENG Kun, WANG Xiao-meng, DING Bao-ting, et al. *Acidithiobacillus ferrooxidans* mediates morphology evolution of schwertmannite in the presence of Fe^{2+} [J]. Chemical Geology, 2022, 598: 120828. DOI: 10.1016/j.chemgeo.20.120828.

[9] PECHISHCHEVA N V, ESTEMIROVA S K, KIM A V, et al. Adsorption of hexavalent chromium on mechanically activated graphite [J]. Diamond and Related Materials, 2022, 127: 10915. DOI: 10.1016/j.diamond.20.10915.

[10] LIU Hai-yan, GUO Hua-ming, POURRET O, et al. Geochemical signatures of rare earth elements and yttrium exploited by acid solution mining around an ion-adsorption type deposit: Role of source control and potential for recovery [J]. Science of the Total Environment, 2022, 804: 150241. DOI: 10.1016/j.scitotenv.2021.150241.

[11] ASHOUR R M, EL-SAYED R, ABDEL-MAGIED A F, et al. Selective separation of rare earth ions from aqueous solution using functionalized magnetite nanoparticles: Kinetic and thermodynamic studies [J]. Chemical Engineering Journal, 2017, 327: 286−296. DOI: 10.1016/j.cej.2017.06.101.

[12] YAN Qiu-ting, YANG Ya-lin, CHEN Wei, et al. Recovery and removal of rare earth elements from mine wastewater using synthesized bio-nanoparticles derived from Bacillus cereus [J]. Chemical Engineering Journal, 2023, 459: 141585. DOI: 10.1016/j.cej.20.141585.

[13] EL OUARDI Y, LAMSAYAH M, BUTYLINA S, et al. Sustainable composite material based on glutenin biopolymeric-clay for efficient separation of rare earth elements [J]. Chemical Engineering Journal, 2022, 440: 135959. DOI: 10.1016/j.cej.20.135959.

[14] REN Jing-jing, ZHENG Liu-chun, SU Yao-ming, et al. Competitive adsorption of Cd(II), Pb(II) and Cu(II) ions from acid mine drainage with zero-valent iron/phosphoric titanium dioxide: XPS qualitative analyses and DFT quantitative calculations [J]. Chemical Engineering Journal, 2022, 445: 136778. DOI: 10.1016/j.cej.20.136778.

[15] JAVADIAN H, RUIZ M, SALEH T A, et al. Ca-alginate/carboxymethyl chitosan/$Ni_{0.2}Zn_{0.2}Fe_{2.6}O_4$ magnetic bionanocomposite: Synthesis, characterization and application for single adsorption of Nd^{+3}, Tb^{+3} and Dy^{+3} rare earth elements from aqueous media [J]. Journal of Molecular Liquids, 2020, 306: 112760. DOI: 10.1016/j.molliq.2020.112760.

[16] SMITH Y R, BHATTACHARYYA D, WILLHARD T, et al. Adsorption of aqueous rare earth elements using carbon black derived from recycled tires [J]. Chemical Engineering Journal, 2016, 296: 102−111. DOI: 10.1016/j.cej.2016.0.08.